Unidimensional simulation of radiative transport of electronic energy

E.J. Nunes Pereira, M.N. Berberan-Santos, J.M.G. Martinho

Centro de Química-Física Molecular, Instituto Superior Técnico, 1096 Lisboa Codex, Portugal

Abstract

The radiative transport of electronic energy is simulated in one dimension by stochastic methods (homogeneous Markov chains and Monte Carlo simulation). This approach allows the calculation of the fluorescence decay curves as a function of both the excitation and the emission wavelengths and of the fluorescence spectrum for given concentration, excitation/emission geometry and photophysical characteristics of the fluorophore. Time-resolved fluorescence and steady-state spectra of 9,10-diphenylanthracene (DPA) in benzene at several concentrations for front-face, right-angle and transmission geometries were calculated and compared with the available experimental results.

1. Introduction

The fluorescence and absorption spectra of fluorophores often overlap. This creates the possibility of electronic energy transfer between identical molecules (energy transport or energy migration), which occurs by both radiative and nonradiative

luminescence of high-pressure discharge lamps [7], luminescent solar concentrators [8] and stellar atmospheres [9]. The radiative mechanism occurs by reabsorption of the fluorescence in successive steps and can be described by Scheme 1 [7, 10–12].

In Scheme 1, A_1 are the primarily excited molecules by the incoming beam of radiation and A_n
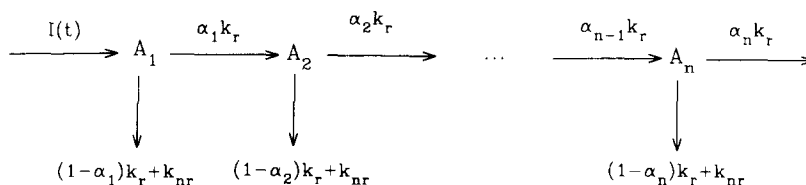
Scheme 1. The radiative mechanism.

mechanisms usually operating in parallel [1]. The nonradiative process has been the subject of many studies after the pioneer works of Perrin [2], Perrin [3] and Förster [4, 5], while the radiative one has been less considered notwithstanding its importance in solid state and dye lasers systems [6],

($n > 1$) are the successive generations of molecules created by reabsorption of the emitted light in the medium. The parameter α_n is the average probability of reabsorption for a photon emitted by the nth-generation molecules A_n, and k_r, k_{nr} are the deactivation radiative and nonradiative rate

constants, respectively. Neglecting correlations between the reabsorption processes the kinetic scheme yields, for a δ-pulse excitation [7, 10–12]

$$A_n = A_0 a_{n-1} \frac{(k_r t)^{n-1}}{(n-1)!} \exp\left(-\frac{t}{\tau_0}\right), \tag{1}$$

with

$$a_{n-1} = \prod_{i=1}^{n-1} \alpha_i \quad (a_0 = 1) \tag{2}$$

The intensity due to A_n detected in a certain direction and solid angle, I_n, depends on the photon escape probability, $S_n(\lambda)$, and on geometric effects depending on the detecting system, G_n, being given by [11]:

$$I_n(\lambda, t) = G_n S_n(\lambda) k_r A_n(t) \tag{3}$$

and the total intensity is [11]:

$$I(\lambda, t) = \sum_{n=1}^{\infty} I_n(\lambda, t)$$

$$= G k_r A_0 \exp\left(-\frac{t}{\tau_0}\right) \sum_{n=1}^{\infty} S_n(\lambda) a_{n-1} \frac{(k_r t)^{n-1}}{(n-1)!}, \tag{4}$$

where $G_n = G$ is considered independent of the generation of excited molecules.

The assumptions made in the derivation of the above equations were already discussed by Martinho et al. [11]. Nevertheless, it should be emphasized again that implicit in Eqs. (1)–(4) is the neglect of nonradiative transport. Although radiative and nonradiative transport can operate in parallel since they both depend on the overlap integral between fluorescence and absorption spectra, the decay law (and hence, the steady-state emission) is not changed by nonradiative transport [4]. However, the nonradiative mechanism could change the spatial distribution functions of the A_n molecules and therefore change the decay due to the change of the optical path over which the radiation can be reabsorbed. This effect is negligible when compared to the spread of excitation due to radiative transport as can be seen when one con-

siders the diffusion coefficient for excitation migration ($D \approx 1.4 \times 10^{-5}$ cm^{2}s^{-1} for DPA–DPA transport in a 5×10^{-2} M solution in benzene which corresponds to only 2.9×10^{-6} cm spread of excitation after 100 ns [11]).

Decay curve measurements on systems where radiative transport is important can be well fitted with the decay law (4) [11, 13]. This fit allows, in principle, the determination of the absorption coefficients, which should be compared with the analytical values predicted by the radiative transport model. However, this verification is limited by both the complexity of the analytical calculation of the reabsorption coefficients and by the experimental feasibility of extracting from the fit more than two coefficients with reasonable accuracy [11]. To overcome these problems, Monte Carlo simulation and the homogeneous Markov Chain method are used to simulate the unidimensional radiative transport for both front-face, transmission and right-angle viewing geometries. Both methods allow the calculation of reabsorption coefficients, escape probabilities, decay curves at several emission wavelengths and fluorescence spectra once the excitation wavelength, concentration, excitation/emission geometry and molecular parameters of the fluorophore (fluorescence and absorption spectra, molecular quantum yield and lifetime) are known. The values obtained from the simulation are compared with published results from the literature.
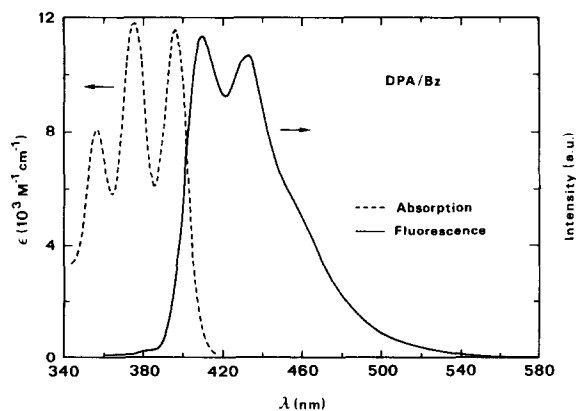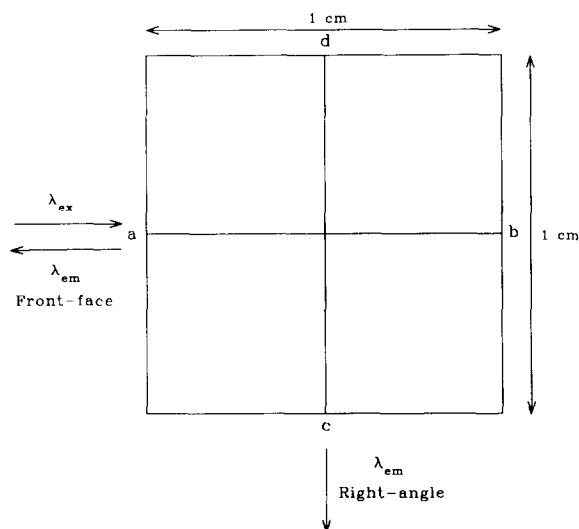

Fig. 1. Molecular fluorescence (——) and absorption (---) spectra of DPA in benzene.

2. Stochastic simulation

Scheme 2 shows the excitation/emission geometries considered in the unidimensional simulation used to predict the fluorescence spectra and decay curves.

Scheme 2. The excitation/emission geometries considered in the unidimensional simulation and used to predict the fluorescence spectra and decay curves.

The radiative transport along segment [a,b] simulates a front-face or a transmission geometry (depending if the emission is detected from the same or the opposite side to the excitation side), while the right-angle viewing is simulated when radiative transport occurs along segment [c,d].

For both front-face and transmission geometries the initial excited molecules were distributed along segment [a,b] following Beer's law, while for right-angle viewing a δ-distribution of excited molecules in the middle of the cell was used, which is also a consequence of Beer's law (see Scheme 2).

The real molecular system chosen was 9,10-diphenylanthracene (DPA) in benzene owing to the existence of extensive experimental evidence of reabsorption effects on this system [11,14] and of a substantial overlap between the fluorescence and absorption spectra as shown in Fig. 1. Moreover, this compound seems ideal to test the radiative transport model since it does not exhibit excimer

formation nor concentration quenching of its fluorescence (due to steric hindrance by the phenyl groups [1]), which could otherwise disguise the influence of the radiative mechanism over experimental data of concentrated solutions.

Both the Monte Carlo simulation and homogeneous Markov chains methods can be used for the simulation. In either method, the simulation is performed in order to calculate sequentially the distribution functions of excited molecules, the reabsorption probabilities, decay curves and fluorescence spectrum. However, the homogeneous Markov chains method generates smoother distribution functions and is less computer-time consuming. This was therefore the method of choice although, for comparison, some results were also obtained by the Monte Carlo method as described in Appendix A.

The homogeneous Markov chains describe stochastic processes that evolve in time remembering only the most recent past (Markov property) and whose conditional distributions are time invariant (homogeneity) [15]. These conditions are fulfilled in the case of radiative transport provided the probability of reabsorption of a photon by a given molecule and in a given coordinate is independent of the generation to which the molecule belongs. In this case, the nth-generation distribution function of excited molecules, described by the column vector $\mathbf{p}^{(n)}$, whose elements are the positional probabilities $p_i^{(n)} = p^{(n)}(x_i)$, is simply calculated from the previous one by the recursive formula

$$\mathbf{p}^{(n)} = \mathbf{P}\mathbf{p}^{(n-1)} \tag{5}$$

where P is the transition matrix whose elements are the step transition probabilities. Once the vector $\mathbf{p}^{(1)}$ of the initial distribution of excited molecules is known, the subsequent distribution functions are straightforwardly calculated by successive application of expression (5). The elements of the vector $\mathbf{p}^{(1)}$ are, for both front-face and transmission geometries, given by

$$p_1^{(1)} = 0,$$

$$p_i^{(1)} = \mu(\lambda_{\mathrm{exc}})c \exp\left\{-\mu(\lambda_{\mathrm{exc}})cx_i\right\}h, \ i \in \{2,\ldots,m+1\},$$

$$p_{m+2}^{(1)} = \exp\{-\mu(\lambda_{\mathrm{exc}})cl_{\mathrm{max}}\}, \tag{6}$$

where m (1024) is the number of sub-intervals in which the cell of length l_{max} is divided, x_i the mean coordinate of sub-interval i, h the length of each sub-interval, c the concentration and, $\mu(\lambda) = \ln 10 \varepsilon(\lambda)$, $\varepsilon(\lambda)$ being the molar absorption co-efficient. The square transition matrix

$$\mathbf{P} = \begin{bmatrix} 0 & p_{21} & p_{31} & \cdots & p_{m+1,1} & 0 \\ 0 & p_{22} & p_{32} & \cdots & p_{m+1,2} & 0 \\ 0 & p_{23} & p_{33} & \cdots & p_{m+1,3} & 0 \\ \vdots & \vdots & \vdots & \vdots & \vdots & \vdots \\ 0 & p_{2,m+2} & p_{3,m+2} & \cdots & p_{m+1,m+2} & 0 \end{bmatrix} \quad (7)$$

has zero elements on the first and last columns, corresponding to the exit of the photon to the left and right sides of the cell, the others elements being given by

$$p_{ij} = \int_{\lambda_{min}}^{\lambda_{max}} \tfrac{1}{2} F(\lambda) p_{ij}(\lambda)\, d\lambda, \quad (8)$$

where the integral is performed over the fluorescence-absorption overlap defined by the wavelengths λ_{min} and λ_{max}, the factor $\tfrac{1}{2}$ taking into account the probability of the emission being directed to the right or to the left sides and

$$p_{ij}(\lambda) = \mu(\lambda) c \exp\{-\mu(\lambda) c d_{ij}\} \times h \qquad \forall i,j \neq 1, m+2 \quad (9)$$

gives the probability of a photon emitted in interval i being absorbed at a distance $d_{ij} = |j - i| h$ in interval j. An extension of this treatment considering a possible reflection at the cell walls is presented in Appendix B. For a normal incidence of the light in the silica surface (reflectivity $\approx 4\%$) the effect of reflection by the cell walls on the simulated decay curves and fluorescence spectra is very small.

Fig. 2 shows the normalized distribution functions of several generations of excited molecules obtained by homogeneous Markov chains for a 10^{-3} M DPA solution in benzene excited by 337 nm radiation, using a front-face geometry.

The relative number of excited molecules in the successive generations is significant owing to the
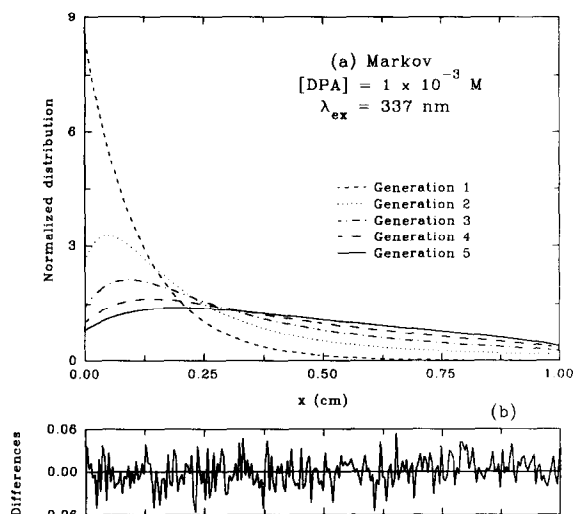

Fig. 2. (a) Normalized distributions functions for several generations of excited molecules obtained by homogeneous Markov chains for a 10^{-3} M DPA solution in benzene excited at 337 nm using front-face viewing geometry: (– – –) 1st generation; (· · ·) 2nd generation; (– · –) 3rd generation; (––) 4th generation; (———) 5th generation. (b) Plot of the differences for the 5th generation of excited molecules obtained by Markov homogeneous chain and Monte Carlo simulation.

substantial overlap between the fluorescence and absorption spectra (see Fig. 1) and also to the high fluorescence quantum yield of DPA in benzene.

The primarily excited molecules distribution function obeys Beer's law while subsequent distribution functions largely deviate from the initial one showing progressively deeper penetration of radiation into the cell as reabsorption proceeds.

Fig. 2 also includes the differences for the distribution functions of the 5th-generation of excited molecules calculated by both the homogeneous Markov chains and the Monte Carlo simulation (Appendix A) methods. The differences are very small and randomly distributed indicating that both methods give equivalent results.

3. Simulated results

Using the procedure described above the influence of concentration, excitation/emission geometry and excitation optical density, can be

studied for a particular fluorophore and the results compared with the experimental observations.

Figs. 2 and 3 show the influence of DPA concentration (compare Fig. 2 with Fig. 3(a), taking care of the difference in x-coordinate scale) and of the excitation wavelength (compare Fig. 3(a) with (b)) on the excited state distribution functions, for front-face viewing.

The increase of concentration has a two-fold effect on the radiative transport process. It leads to larger optical densities at excitation wavelength and as a result the primarily excited molecules are closer to the excitation side. Moreover, since there is also an increase of optical density at emission

wavelengths, the mean optical path of the emitted photons in the medium prior to reabsorption decreases. This results on a lesser spreading of the distribution functions as one goes from one generation to the next. The combined effect of an increase of optical density at both excitation and emission wavelengths results in the excitation being much more concentrated near the face of the cell exposed to excitation. It is important to remark that, because the molar absortivity ε is in general a function of the wavelength, the effect of concentration cannot be reduced to a re-scaling of the results obtained for a given particular concentration. On the other hand, an alteration of the excitation wavelength changes the optical density at the excitation wavelength but not at the emission wavelengths. If, for the same concentration, the optical density is increased (as in going from Fig. 3(a) to (b)), then the primarily excited molecules distribution will change accordingly, becoming closer to excitation side. Although the mean optical path prior to reabsorption (that is, the spreading of excitation in going from one generation to the next) does not change because it only depends on the product εc, the distribution functions of subsequently excited molecules will change (see for instance the distribution function of the 2nd generation molecules) since these depend on the distribution of the first generation molecules, see Eq. (5).

Fig. 4 shows again the distribution function of several generations of excited molecules for DPA in benzene solutions (10^{-3} and 10^{-2} M) but now for right-angle viewing.

The excited molecules occur in this case symmetrically to the left and right sides of the cell with reabsorption, the spread of the initial distribution decreasing again with concentration owing to the decrease of the mean optical path of the emitted photons prior to reabsorption.

Knowing the distribution functions of the excited molecules, the calculation of the reabsorption probability, α_n, is straightforward. Indeed,
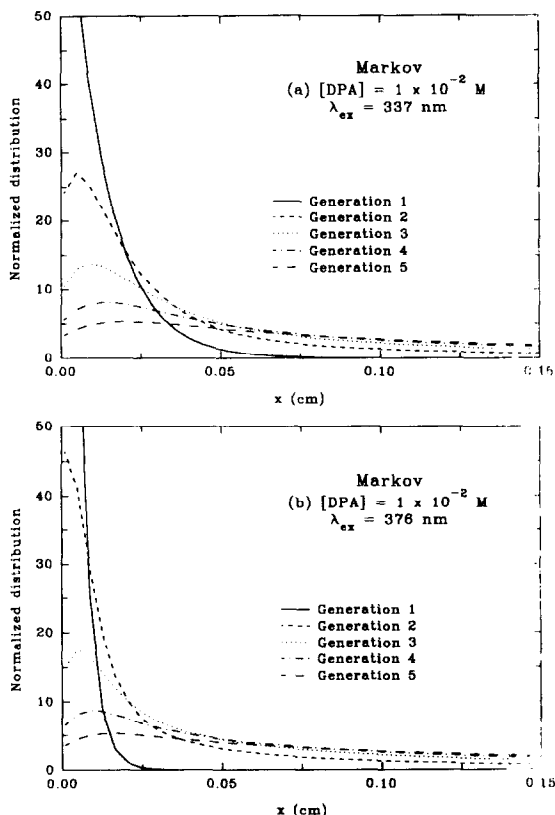

Fig. 3. Normalized distributions functions for several generations of excited molecules obtained by homogeneous Markov chains for 10^{-2} M DPA solution in benzene excited at (a) 337 nm and (b) 376 nm using front-face viewing geometry: (———) 1st generation; (– – –) 2nd generation; (· · ·) 3rd generation; (– · –) 4th generation; (— — —) 5th generation.

$$\alpha_n = \int F(\lambda) p_n(\lambda) \, d\lambda \tag{10}$$

where $F(\lambda)$ is the normalized fluorescence spectrum (the area of the spectrum is unitary and its shape
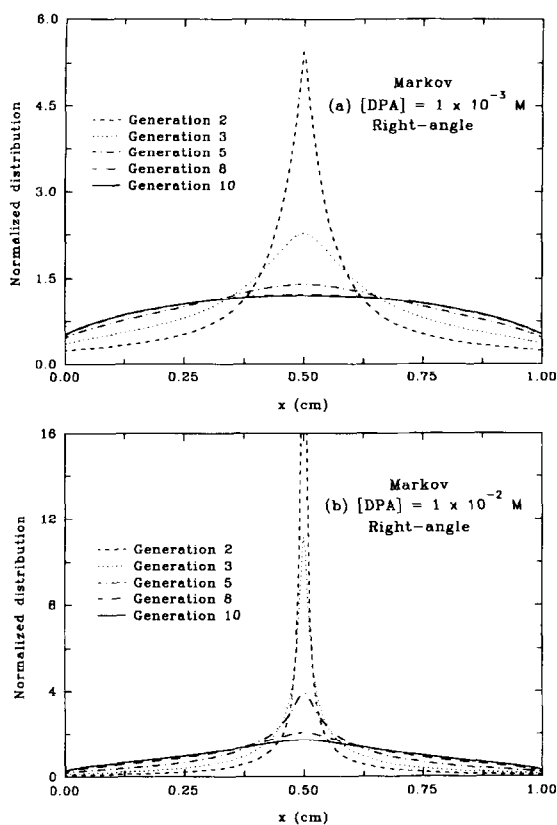
Fig. 4. Normalized distributions functions for several generations of excited molecules obtained by homogeneous Markov chains for (a) 10^{-3} M and (b) 10^{-2} M DPA solution in benzene using right-angle viewing geometry: (– – –) 2nd generation; ($\cdots$) 3rd generation; (– · –) 5th generation; (– –) 8th generation; (———) 10th generation.

$p_n(x)$ being the spatial distribution function of the nth-generation of excited molecules at distance x within the medium. The escape probability from

the left side of the cell is given by

$$S_n^{(l)}(\lambda) = \int_0^{l_{max}} \exp(-\mu cx) p_n(x)\,dx \qquad (12)$$

while from the right side is

$$S_n^l(\lambda) = \int_0^{l_{max}} \exp[-\mu c(l_{max} - x)] p_n(x)\,dx \qquad (13)$$

From Eq. (3) it is now possible to calculate the contribution to the decay of each generation of excited molecules. Fig. 5 show the fluorescence decay ($\lambda = 400$ nm) of a 10^{-2} M solution of DPA in benzene excited at 337 nm using a front-face viewing.

For early times the main contribution to the decay comes from the initially excited molecules, adding the following generations of excited molecules small contributions whose importance diminishes with the generation number. The initially excited molecules decay exponentially, but the following generations of molecules have an initial rise component decaying afterwards after passing through a maximum. This is the expected time

identical for all generations of excited molecules) and $p_n(\lambda)$ the spatial average probability of reabsorption of a photon emitted by the nth-generation molecules

$$p_n(\lambda) = \int_0^{l_{max}} \frac{1}{2} \{2 - \exp(-\mu cx) - \exp[-\mu c(l_{max} - x)]\}$$
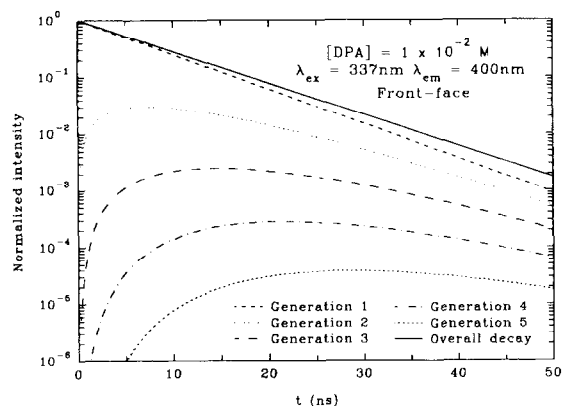
$$\times p_n(x)\,dx \qquad (11)$$

Fig. 5. Contribution of several generations of excited molecules to the overall observed decay observed at 400 nm for a 10^{-2} M solution of DPA in benzene excited at 337 nm using front-face viewing: (– – –) 1st generation; ($\cdots$) 2nd generation; (— —) 3rd generation; (– · –) 4th generation; (– – – –) 5th generation; (———) overall decay curve. The overall decay includes the contribution of 15 generations of excited molecules.

evolution of the excited molecules since excluding the primarily excited molecules all others are created with a time delay from the excitation time by the reabsorption process.

Fig. 6 shows the decay curve of the same solution obtained at several wavelengths in the reabsorption region.

The decay is emission wavelength dependent in the reabsorption region (see Eq. (4)) owing to the decrease of the $S_n(\lambda)/S_1(\lambda)$ ratio with n which is in turn a result of the deeper penetration of the radiation into the cell as reabsorption proceeds. The fastest decay occurs at wavelengths where DPA absorption is maximum owing to a larger decrease of $S_n(\lambda)/S_1(\lambda)$ ratio with n when DPA absorption is higher.

The decay is complex (see Eq. (4)) and can not of course be fitted by a single exponential as should be in the absence of reabsorption. For comparison with the experimental results, the mean radiative lifetime is defined by

$$\tau(\lambda) = \frac{\int_0^\infty t \times I(\lambda, t)\, \mathrm{d}t}{\int_0^\infty I(\lambda, t)\, \mathrm{d}t} = \left\{ \sum_{n=1}^\infty n\, \Theta_n(\lambda) \right\} \tau_0 \qquad (14)$$

where

$$\Theta_n(\lambda) = \frac{\int_0^\infty I_n(\lambda, t)\, \mathrm{d}t}{\int_0^\infty I(\lambda, t)\, \mathrm{d}t} = \frac{S_n(\lambda)\, a_{n-1}\, \Phi_0^{n-1}}{\sum_{n=1}^\infty S_n(\lambda)\, a_{n-1}\, \Phi_0^{n-1}} \qquad (15)$$

is the relative contribution of the nth generation emission to the overall observed decay.

The predicted mean lifetimes, computed from Eq. (14), are higher than the molecular DPA lifetime owing to the imprisonment of the radiation within the medium. The average lifetimes of DPA in benzene at 430 nm obtained in front-face viewing from both the experimental decays [11] and from
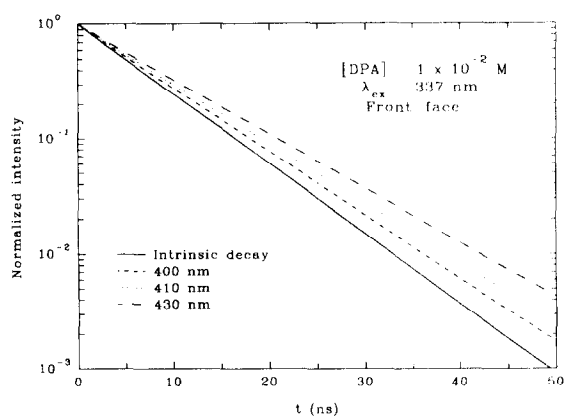

Fig. 6. Normalized decay curves of a 10^{-2} M solution in benzene excited at 337 nm using front-face viewing for several emission wavelengths: (———) intrinsic decay curve; (- -) $\lambda_{em} = 400$ nm; (· · ·) $\lambda_{em} = 410$ nm; (— — —) $\lambda_{em} = 430$ nm. The decays include the contribution of 15 generations of excited molecules.

Eq. (14) (in parenthesis) are very close: 8.6 ns (8.62) at 10^{-3} M ; 9.5 ns (9.11) at 10^{-2} M and 10.3 ns (9.23) at 5×10^{-2} M, all the results corresponding to a 337 nm excitation wavelength.

It is in general observed that the average lifetime for a given concentration increases with wavelength until reabsorption is negligible reaching a constant value afterwards; also the average lifetime for a given fixed wavelength increases with concentration. These were the trends experimentally observed [11].

As a corollary of the discussion of the effect of excitation wavelength on the spatial distribution of excited molecules, it is concluded that the fluorescence decay should also depend on the excitation wavelength, a fact, as far as we know, never clearly stated in the literature. Indeed, that seems to be the case since our simulation results predicts a change from 7.62 ns ($\lambda_{ex} = 376$ nm) to 7.83 ns ($\lambda_{ex} = 337$ nm) for a 10^{-2} M solution of DPA in benzene observed at 400 nm. This is the trend we would expect since, for a given concentration, the higher the penetration of primary excitation into the cell, the more important the radiative transport. There is still a lack of experimental data on the dependence of the decay on λ_{ex} for concentrated solutions.

Fig. 7 shows the contribution to the decay of several generations of molecules for a right-angle viewing geometry of a 10^{-2} M solution of DPA in benzene the fluorescence being recovered at 400 nm.

The contribution to the decay of the several generations of molecules is different from the one observed in a front-face geometry since both the reabsorption probabilities, α_n, and the escape probabilities, $S_n(\lambda)$, are geometry dependent. The influence of the emission wavelength is particularly important for this geometry. Indeed, as shown in Figs. 7 and 8 the decays at wavelengths where DPA absorption is high contain a rise component which is not observed for longer wavelengths where reabsorption is smaller.

This behavior observed in right-angle geometry but never observed for front-face viewing is due to the large contribution of high generations of excited molecules to the decay since the emission of the primarily excited molecules is strongly absorbed. This certainly is the explanation for the rise component detected in the experimental decays of rhodamine B [12] and rhodamine 575 [8].

The reasoning that was used to explain the dependence of the radiative transport on the excita-

Fig. 8. Normalized decay curves of a 10^{-2} M solution in benzene using right-angle viewing for several emission wavelengths: (———) intrinsic decay curve; ($\cdot\cdot\cdot$) $\lambda_{em} = 400$ nm; (— — —) $\lambda_{em} = 410$ nm; (- -) $\lambda_{em} = 430$ nm. The decays include the contribution of 15 generations of excited molecules.

tion wavelength for front-face measurements applies equally well for the right-angle geometry. This means that the decay (and hence, the mean lifetimes and the steady-state emission) should also depend on λ_{ex}, the dependence being higher the greater the optical density at excitation wavelength. However, we are not able to account for this dependence in our unidimensional approximation of the 3D real cell since a δ-distribution was always used for the first generation of excited molecules, irrespective of the value of λ_{ex} (see Section 2). The reason for this procedure was the following (see Scheme 2): although the molecules A_1 are distributed along the excitation direction (segment [a,b]) according to the Beer law, the intersection of the excitation direction with segment [c,d] (the segment used in the unidimensional simulation for the right-angle geometry) is only the central point of the cell. Since we are mainly concerned with the normalized distribution of the A_1 molecules along segment [c,d], this is given by a δ-function irrespective of the optical density at excitation (this of course assumes that the optical density at the excitation wavelength is low enough so that the external excitation is able to reach the middle of the cell). Tough only a tridimensional simulation (much more demanding in computation time) will account for the fluorescence data dependence on the optical density at
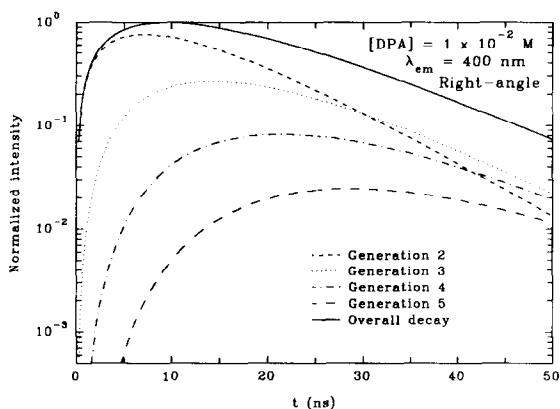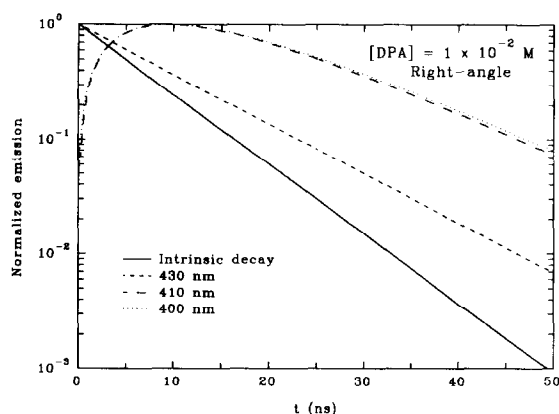

Fig. 7. Contribution of several generations of excited molecules to the overall observed decay observed at 400 nm for a 10^{-2} M solution of DPA in benzene using front-face viewing: (———) 2nd generation; ($\cdot\cdot$) 3rd generation; (- · -) 4th generation; (— — —) 5th generation; (———) overall decay curve. The overall decay includes the contribution of 15 generations of excited molecules.

excitation wavelength, the unidimensional model is nevertheless important since it conveys a simple (tough admittedly crude) description of the essential features of the physical process in right-angle and, in particular, is able to predict a rise-time in time-resolved fluorescence provided the reabsorption at emission wavelengths is high enough.

The simulated fluorescence spectrum of a fluorophore is directly available from the decay curves at several emission wavelengths. Indeed,

$$I(\lambda) = \int_{0}^{\infty} I(\lambda, t)\,\mathrm{d}t, \qquad (16)$$

with $I(\lambda, t)$ given by Eq. (4).

Fig. 9 shows the simulated fluorescence spectra of DPA solutions in benzene for a front-face viewing geometry.

The shape of the simulated spectrum changes with concentration, the fluorescence intensities being reduced in the reabsorption region and enhanced at longer wavelengths where reabsorption is absent. Fig. 10 shows the simulated fluorescence spectra of a 10^{-2} M DPA solution in benzene using both front-face and transmission geometries.

Although the spectral distortion due to reabsorption is well known, the simulated spectra in Figs. 9 and 10 can be used to illustrate the dangers associated with relative determinations of fluorescence quantum yields of concentrated solutions.

The fluorescence quantum yield is of course unambiguously defined as the ratio of number of emitted photons over number of absorbed photons. The presence of radiative transport in concentrated solutions renders this value different from the molecular quantum yield; the quantum yield in the presence of reabsorption must be lower than the molecular value since in each reabsorption–reemission event the average probability $1 - \Phi_0$ of nonradiative decay reduces the number of photons that can eventually be detected. However, the possibility of reabsorption allied with the occurrence of highly inhomogeneous spatial distributions of excited species makes the steady-state spectrum very sensitive on the collecting geometry as can easily be seen in Fig. 10. Even tough the front-face and transmission
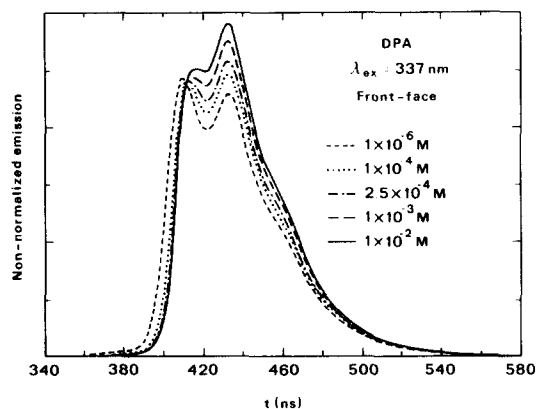

Fig. 9. Fluorescence spectra of several solutions of DPA in benzene excited at 337 nm using front-face viewing: (– – –) 10^{-6} M; (· · ·) 10^{-4} M; (– · –) 2.5×10^{-4} M; (— — —) 10^{-3} M; (———) 10^{-2} M.
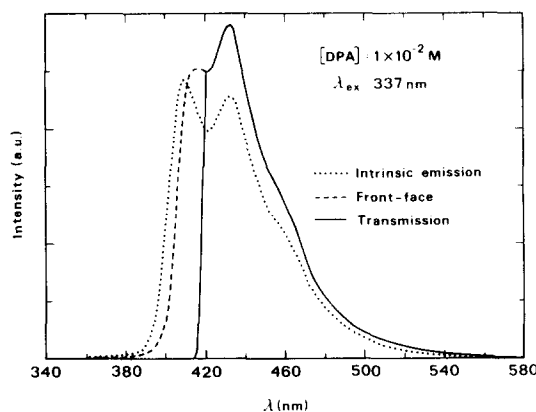

Fig. 10. Intrinsic fluorescence spectrum (· · ·) and technical fluorescence spectra in front-face (— — —) and transmission (———) geometries for 10^{-2} M solution of DPA in benzene excited at 337 nm.

spectra are for the same solution with the same excitation optical density (and hence, correspond to the same fluorescence quantum yield), the areas under the steady-state emission are quite different. This shows that the error associated with the use of the area under the steady-state emission collected in only one of these geometries for the purpose of estimating the quantum yield can be significant. Unless one makes a 4π spatial integration of the fluorescence emission to calculate relative quantum

yields, the area under the spectrum is not a good approximation of the real quantum yield and will be termed from now on a technical "quantum yield" [14].

The normalized area to the same number of initially excited molecules can be greater or lower than the area of the molecular spectrum, depending on the geometry. Indeed, owing to reabsorption the fluorescence of the initial excited molecules is only partially detected but as the emission occurs in all directions some of the photons emitted in other directions can be subsequently detected counterbalancing or not the initial photons lost. This is illustrated in Fig. 11 where the quantum yield[t] (counting the emitted photons in all directions) and the technical "quantum yields" (measured by the area of the fluorescence spectra) versus concentration are plotted for both front-face and transmission geometries.

The technical "quantum yields" obviously do not have physical meaning and deviate themselves more from the real value the higher the concentration. The technical "quantum yield" in front-face (usually used in measurements of concentrated solutions) is higher than the molecular quantum yield ($\Phi_0 = 0.955$ [16]) and can be even larger than one at high concentrations. On the other hand, the values in transmission are always lower than Φ_0 decreasing with concentration. The real quantum yield is slightly lower than Φ_0 owing to the small importance of the nonradiative processes in DPA whose molecular quantum yield is very close to unity (0.955). These observations have experimental confirmation on the experimentally observed increased of "quantum yield" of DPA [14] with concentration for front-face geometry. Experimental quantum yields for transmission geometry are rare, even so Kilin and Rozman [10] observed a decrease in "quantum yield" with concentration for several organic scintillators in a matrix of polystyrene.
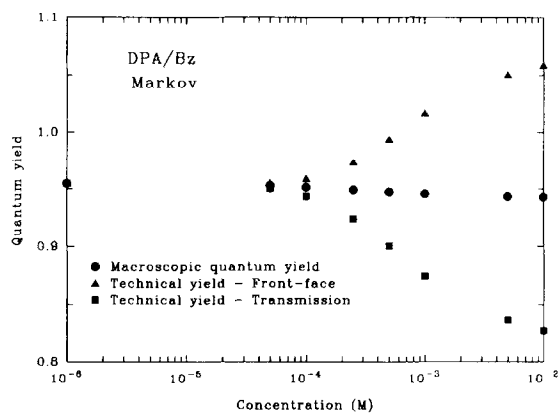

Fig. 11. Quantum yields of DPA solutions in benzene when excited at 337 nm: (●) macroscopic quantum yield; (▲) technical "quantum yield" for front-face geometry; (■) technical "quantum yield" for transmission geometry.

4. Conclusions

The radiative transport proceeding through a trivial mechanism of successive steps of reabsorption of the emitted light, is difficult to modelize. Indeed, the dependence on geometry introduces great complexity, hindering the calculation of exact analytical expressions for the decay curves and fluorescence spectra. The use of Monte Carlo or Markov chains simulation methods is shown to be very appropriate for the calculation of both the decay curves and fluorescence spectra once the geometry and the fluorophore properties are known. The unidimensional model given here is a simplification of the real radiative transport occurring in two or three-dimensional medium. Nevertheless, some qualitative trends could be extracted and the comparison made with experimental results was surprisingly good. Work to extend the simulations to three dimensions is currently under progress.

[t] The quantum yield can also be termed macroscopic (to differentiate it from the intrinsic, molecular quantum yield in the absence of reabsorption or concentration quenching) or real (to differentiate it from the technical "quantum yield" given by the area under the spectrum in one particular geometry, which is only an operational parameter) yield.

Appendix A. Monte Carlo simulation

The radiative transport of electronic energy is intrinsically a random process since the occurring events within the medium (probabilities of emission at a given wavelength, direction of emission, photon absorption and length traveled by the emitted photon) are random quantities with known distribution functions. These were generated by the transformation method (see bellow) from a pseudo random number generator uniform in the interval [0,1[. The simulation process was done step by step. The length of the cell (1 cm length) was divided in 240 intervals and the simulation process begins with the generation of excited molecules obeying Beer's law (front-face and transmission viewing) or δ-spiking in the middle of the cell (right-angle viewing). The trajectory of the excitation within the cell is then generated using random numbers with appropriate distribution functions characteristic of the different processes that can occur to the photon. In order to obtain reliable values the procedure was repeated many times and stopped when 500000 counts were obtained for the 5th-generation of excited molecules.

The generation of nonuniform variables from a uniform variable is done by a transformation [17]. Indeed, if the normalized density of probability $f(x)$ to which the random variable must obey is known, x given by

$$x(r) = F^{-1}(r),\qquad(A1)$$

where

$$F(x) = \int_{-\infty}^{x} f(u)\,du\qquad(A2)$$

has the desired distribution being r a uniform variable in [0,1[. For instance, to calculate the probability of reabsorption the random variable $x(r)$ is given by

$$x(r) = -\frac{\ln(1-r)}{\mu(\lambda)c},\qquad(A3)$$

since the probability of reabsorption of the fluorescence light of wavelength λ at a distance x from the emission point has a probability density (Beer's law)

$$f(x) = \mu(\lambda)c \exp\{-\mu(\lambda)cx\},\qquad(A4)$$

where c is the concentration and $\mu(\lambda)c = 2.303\varepsilon(\lambda)$, $\varepsilon(\lambda)$ being the molar absorption coefficient.

Appendix B. Transition matrix considering reflection by the cell walls

The reflection of the emitted light on the surface of the cell walls introduces the possibility of other reabsorption–reemission events. The transition probability considering the probability $p_{ij}(\lambda)$ considering the probability r of occurring reflections in the cell walls is given by

$$p_{ij}(\lambda) = \mu c e^{-\mu c d_{ij}} \times h +$$

$$r \times e^{-\mu c x_i} \times \{[\mu c e^{-\mu c x_j}] \times h$$

$$+ [(e^{-\mu c l_{max}} \times r)^2 \times \mu c e^{-\mu c x_j}] \times h + \dots\} +$$

$$r \times e^{-\mu c x_i} \times \{[(e^{-\mu c l_{max}} \times r) \times \mu c e^{-\mu c (l_{max} - x_j)}] \times h$$

$$+ [(e^{-\mu c l_{max}} \times r)^3 \times \mu c e^{-\mu c (l_{max} - x_j)}] \times h + \dots\}$$

$$r \times e^{-\mu c (l_{max} - x_i)} \times \{[\mu c e^{-\mu c (l_{max} - x_j)}]$$

$$\times h + [(e^{-\mu c l_{max}} r)^2$$

$$\times (\mu c e^{-\mu c (l_{max} - x_j)})] \times h + \dots\} +$$

$$r \times e^{-\mu c (l_{max} - x_i)} \times \{[(e^{-\mu c l_{max}} \times r)$$

$$\times (\mu c e^{-\mu c x_j})] \times h + [(e^{-\mu c l_{max}} r)^3$$

$$\times (\mu c e^{-\mu c x_j})] \times h + \dots\}$$

which can be understood with the help of the diagram of the cell optical path
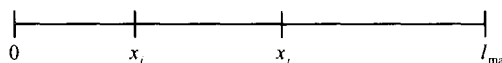
The first line gives the contribution due to direct absorption prior to reflection. The others ones give the absorption probabilities in segment j given that the light was emitted from segment i to the left side (2nd and 3rd lines) or to the right side (4th and 5th lines), after occurring at least one reflection in the

cell walls. The 2nd and 5th lines consider the photon absorption events occurring in segment j coming from the left side while the 3rd and 4th lines the ones coming from the right side.

The terms in lines 2 to 5 are the elements of a series and can be rewritten in a condensed form

$$p_{ij}(\lambda) = \mu c e^{-\mu c d_{ij}} \times h \,+$$

$$r \times e^{-\mu c x_i} \times \left\{ \sum_{n=0}^{\infty} (r \times e^{-\mu c l_{max}})^{2n} \right\} \times (\mu c e^{-\mu c x_j}) \times h \,+$$

$$r \times e^{-\mu c x_i} \times \left\{ \sum_{n=0}^{\infty} (r \times e^{-\mu c l_{max}})^{2n+1} \right\}$$

$$\times (\mu c e^{-\mu c(l_{max} - x_j)}) \times h \,+$$

$$r \times e^{\mu c(l_{max} - x_i)} \times \left\{ \sum_{n=0}^{\infty} (r \times e^{-\mu c l_{max}})^{2n} \right\}$$

$$\times (\mu c e^{-\mu c(l_{max} - x_j)}) \times h \,+$$

$$r \times e^{-\mu c(l_{max} - x_i)} \times \left\{ \sum_{n=0}^{\infty} (r \times e^{-\mu c l_{max}})^{2n+1} \right\} \times (\mu c e^{-\mu c x_j}) \times h.$$

Note that each element of the series is related with the number of times that the radiation travels the cell path length without being absorbed. Performing the summation,

$$p_{ij}(\lambda) = \mu c e^{-\mu c |x_j - x_i|} \times h + \frac{r \mu c}{(1 - r e^{-\mu c l_{max}})^2}$$

$$\times \{[e^{-\mu c(l_{max} + x_i - x_j)} + e^{-\mu c(l_{max} - x_i + x_j)}] \quad (B3)$$

$$\times r \times e^{-\mu c l_{max}} + [e^{-\mu c(x_j + x_i)}$$

$$+ e^{-\mu c(2 l_{max} - x_i - x_j)}] \times h$$

The escape probabilities are modified accordingly. For instance, to calculate the escape probability to the left the exponential term in Eq. (12) must be modified to

$$(l - r) \times e^{-\mu c x_i} + \frac{r(1 - r) \times e^{-\mu c l_{max}}}{1 - (r e^{-\mu c l_{max}})^2}$$

$$\times \{r e^{-\mu c(l_{max} + x_i)} + e^{-\mu c(l_{max} - x_i)}\}. \quad (B4)$$

The escape probability to the right side is obtained by substitution of x_i by $(l_{max} - x_i)$ in Eq. (B4). The

initial distribution functions must be also modified accordingly. For a front-face viewing geometry the initial distribution function is given by

$$p_i^{(1)} = \frac{\mu c}{1 - (r \times e^{-\mu c l_{max}})^2}$$

$$\times \{e^{-\mu c x_i} + r \times e^{-\mu c(2 l_{max} - x_i)}\} \times h. \quad (B5)$$

Considering an optical glass with a refractive index of about 1.5 and, since air has an index of 1.0, the reflectivity at normal incidence is 4% [18]. This means that 4% of the incident light is reflected and can be reabsorbed again inside the cell increasing the importance of the reabsorption process. Nevertheless, the consideration of a 4% reflectivity in the simulation has a minor effect on the experimental observables (decay curves and fluorescence spectra). For instance, the predicted mean lifetime for a 10^{-2} M DPA solution, excited at 337 nm, measured at 430 nm increases from 9.06 ns (no reflection) only to 9.10 ns ($r = 4\%$). This 0.5% increase is negligible in face of the experimental uncertainty. However, considering only the reflection at normal incidence is a underestimate of the possible importance of the reflection by the cell walls. Indeed, if we consider a concentrated solution in benzene in front-face and, as the fluorescence is emitted in all directions, 38% of the radiation emitted to the detector side lies outside the critical cone for internal reflection (benzene-air critical angle $\Theta_c = 41°$) and could be totally reflected back to solution at the cell wall [18]. However, owing to the longer optical path, most of this radiation will be reabsorbed in the medium before reaching the wall.

References

[1] J.B. Birks, Photophysics of Aromatic Molecules (Wiley, London, 1970).
[2] J. Perrin, Compt. Rendus 184 (1927) 1097.
[3] F. Perrin, Ann. Chim. Phys. 17 (1932) 283.
[4] Th. Förster, Ann. Phys. 2 (1948) 55.
[5] Th. Förster, Z. Naturf. 4a (1949) 321.
[6] Z. Hasan, N.B. Manson, J. Phys. C 21 (1988) 3351; G. Armagan, B. Di Bartolo, Springer Ser. Opt. Sci. 52 (1986) 35; P. Hammond, R. Nelson, IEEE J. Quantum Electron. QE-16 (1980) 1161; M. Ali, S. Ahmed, K. Mitwally, Appl. Opt. 28 (1989) 3708.

[7] P. Wiorkowski, W. Hartmann, Opt. Commun. 53 (1985) 217.

[8] J.S. Batchelder, A.H. Zewail, T. Cole, Appl. Optics 18 (1979) 3090; J.S. Batchelder, A.H. Zewail, T. Cole, Appl. Opt. 20 (1981) 3733.

[9] F.H. Shu, The Physics of Astrophysics, Vols. I and II (University Science Books, New York, 1991).

[10] S.F. Kilin, I.M. Rozman, Opt. Spectrosc. USSR 6 (1959) 40.

[11] J.M.G. Martinho, A.L. Maçanita, M.N. Berberan-Santos, J. Chem. Phys. 90 (1989) 53.

[12] Y. Sakai, M. Kawahigashi, T. Minami, T. Inoue, S. Hirayama, J. Lumin. 42 (1989) 317.

[13] M. Braun, H. Liening, B. Storr, P. Wiorkowski, Opt. Commun. 53 (1985) 221.

[14] J.B. Birks, J. Res. Natl. Bur. Stand. A 80 (1976) 389; W.H. Meluish, J. Phys. Chem. 65 (1961) 229.

[15] M. Iofescu, Finite Markov Processes and Their Applications (Wiley, New York, 1980); A.T. Bharucha-Reid, Elements of the Theory of Markov Processes and Their Applications (McGraw-Hill, New York, 1960).

[16] S.R. Meech, D. Phillips, J. Photochem. 23 (1983) 193.

[17] W.H. Press, B.P. Flannery, S.A. Teukolsky, W.T. Vetterling, Numerical Recipes, The Art of Scientific Computing (Cambridge University Press, Cambridge, 1986).

[18] R. Guenther, Modern Optics (Wiley, New York, 1990).